Solid Earth Discuss., 6, 3075–3109, 2014
www.solid-earth-discuss.net/6/3075/2014/
doi:10.5194/sed-6-3075-2014

Solid Earth
Discussions
Open Access

Polyphase evolution of Pelagonia (northern Greece) revealed by geological and fission-track data

F. L. Schenker[1,2], M. G. Fellin[1], and J.-P. Burg[1]

[1]Department of Earth Sciences, ETH Zurich, Sonneggstrasse 5, 8092 Zurich, Switzerland
[2]Institute of Earth Sciences, University of Lausanne, 1015 Lausanne, Switzerland

Received: 2 October 2014 – Accepted: 6 October 2014 – Published: 10 November 2014

Correspondence to: F. L. Schenker (filippo.schenker@unil.ch)

Published by Copernicus Publications on behalf of the European Geosciences Union.

Abstract

The Pelagonian zone, between the External Hellenides/Cyclades to the west and the Axios/Vardar/Almopia zone (AVAZ) and Rhodope to the east, was involved in late Early Cretaceous and in Late Cretaceous-Eocene orogenic events whose duration are still controversial. This work constrains their late thermal imprints. New and previously published zircon (ZFT) and apatite (AFT) fission-track ages show cooling below 240 °C of the metamorphic western AVAZ imbricates between 102 and ~~93~~–90 Ma, of northern Pelagonia between 86 and 68 Ma, of the eastern AVAZ at 80 Ma and of western Rhodope at 72 Ma. At the regional scale, this heterogeneous cooling is coeval with subsidence of Late Cretaceous marine basin(s) that unconformably covered since 100 Ma the Early Cretaceous (130–110 Ma) thrust system. Thrusting restarted at 70 Ma in the AVAZ and migrated across Pelagonia to reach the External Hellenides at 40–38 Ma. Renewed thrusting in Pelagonia is attested at 68 Ma by abrupt and rapid cooling below 240 °C and erosion of the basement rocks. ZFT and AFT in western and eastern Pelagonia, respectively, set at 40 Ma the latest thermal imprint related to thrusting. Central-eastern Pelagonia cooled rapidly and uniformly from 240 to 80 °C between 24 and 16 Ma in the footwall of a major extensional fault. Extension started even earlier, at 33 Ma in the western AVAZ. Post-7 Ma rapid cooling is inferred from inverse modeling of AFT lengths. It occurred while E–W normal faults were cutting Pliocene-to-recent sediment.

1 Introduction

The Pelagonian zone, in northern Greece (Fig. 1a), is a NW–SE trending metamorphic poly-orogenic thrust nappe (cf. Schermer et al., 1990; Kilias et al., 2010; Schenker et al., 2014) overlain by the Permian–Early Jurassic passive margin of the Axios/Vardar/Almopia zone (AVAZ; Bernoulli and Laubscher, 1972). The Pelagonia and AVAZ are exposed between two nappe-complexes with different compressional

histories (Figs. 1a and 2). To the northeast, the Rhodope complex was built up between the Late Jurassic and the Early Cretaceous (references in Burg, 2012). To the southwest, the fold-and-thrust belt of the External Hellenides formed during Eocene-to-Miocene times (Renz and Reichel, 1945). The Pelagonia zone experienced both thrust events (Godfriaux et al., 1988; Schermer, 1993; Schenker et al., 2014) imprinting a complex distribution of low-temperature thermochronometric data (zircon fission-track (ZFT), zircon (U-Th)/He (ZHe), apatite fission-track (AFT) and apatite (U-Th)/He (AHe), Most, 2003; Vamvaka et al., 2010; Coutand et al., 2014). To the north, ZFT ages range between 86 and 48 Ma and AFT ages between 46 and 25 Ma with the younger ages in the west. To the south ZFT ages range between 76 and 32 Ma, ZHe between 53 and 20 Ma, AFT ages between 42 and 8 Ma and AHe between 26 and 6 Ma with the younger ages in the east (Fig. 1). Integrated into a geological and structural frame, these largely-distributed low-temperature (from 240 to 70 °C, Reiners and Brandon, 2006) cooling ages can substantially contribute to the understanding of tectonic processes and their duration in a multi-event orogeny. By integrating sedimentary, metamorphic and structural observations with both published and new AFT and ZFT ages we aimed: (i) to unravel the role of the Pelagonian zone and the adjacent AVAZ in the multi-event history of the Hellenides and (ii) to characterize in space and time the Eocene-to-Miocene cooling into compressional vs. extensional tectonics.

This study identified four major cooling events: (i) post-collisional, Late Cretaceous cooling and subsidence from to ca. 68 Ma as shown by ZFT ages coeval with the development of marine basins; cooling was heterogeneous in time and space over Pelagonia, AVAZ and western Rhodope, (ii) faster cooling and erosion rates during the Late Cretaceous are coincident with increased detritus from Pelagonia into western AVAZ's basins at ca. 68 Ma, (iii) fast 24 to 16 Ma cooling below 240 °C in the footwall of a normal fault in the central-eastern Pelagonia, (iv) post-7 Ma fast cooling below ca. 80 °C coeval with E–W trending normal fault zones in central-eastern Pelagonia.

1.1 Tectonic setting and geological overview

The Pelagonian zone in the Internal Hellenides is delimited by two ophiolitic domains: the AVAZ to the northeast and the Pindos Ophiolites to the southwest (Fig. 1). The Pelagonia block has been detached from southern Eurasia (Anders et al., 2007), together with the lower unit of Rhodope (Schenker et al., 2014), during Gondwana breakup and subsequent opening of the Tethys Ocean. In the late Early Jurassic, plate convergence and N–NE dipping subduction caused the Late Jurassic-to-Early Cretaceous southwestward obduction of an AVAZ segment onto Pelagonia (Bernoulli and Laubscher, 1972). The obducted Late Triassic-to-Cretaceous carbonates and hemipelagic marls, ultramafic rocks and metavolcanites (schematically represented in Fig. 3), are attributed to the Permian–Early Jurassic southwestern passive margin of the Tethys Ocean (Sharp and Robertson, 2006). Subsequent continent-continent collision between Eurasia and Pelagonia (Schenker et al., 2014) was responsible for Early Cretaceous tectono-metamorphic events (Yarwood and Dixon, 1977; Schermer et al., 1990). The imbricated Pelagonian and Vardar rocks were eroded and covered unconformably by transgressive Cenomanian-to-Early Campanian (100 to 80 Ma) limestones passing upwards into Paleocene turbidites (e.g. Mercier and Vergely, 1994; Papanikolaou, 2009). Maastrichtian-Eocene (ca. 70–38 Ma) syn-orogenic mass flows mark the beginning of a second compression event (Fig. 2) that migrated towards the Eocene-to-Miocene (38–ca. 15 Ma) southwest-vergent accretionary system of the External Hellenides (Jacobshagen et al., 1978). Oligocene–Miocene (post 24 Ma) extension (Le Pichon et al., 1979; Brun and Faccenna, 2008) and related fast cooling were attested only in the southeastern Pelagonian margin (Lecassin et al., 2007; Coutand et al., 2014). Basins at the western (Mesohellenic trough) and eastern (Axios basin, Fig. 1) Pelagonian margins were filled with colluvial-proluvial sediments during the Eocene compressional and the Miocene extensional events. Late Miocene to Pleistocene (post 7 Ma) coal and lacustrine sediments locally covered the Pelagonian basement (Koukouzas et al., 1979; Mavridou et al., 2003; Steenbrink et al., 2006).

In the study area (Fig. 4) the regional main foliation and lithological contacts of Pelagonia are mostly sub-horizontal. Bending of the foliation defines a 20-by-20 km^2 dome with southwestern and northeastern flanks steeper than the northern and southern ones (Fig. 5). Metamorphic grade evolves from amphibolite-facies in the core to greenschist-facies close to the flanks of the dome. The eastern flank is covered by thrust sheets of the AVAZ.

The regional top-to-the-SW sense of shear is associated with collision of Pelagonia with Rhodope (Schenker et al., 2014). Discrete shear zones with top-to-the-NE sense-of-shear overprint the former regional foliation. The most prominent top-to-the-E–NE shear zone separates Pelagonia from the AVAZ (Fig. 5) and contains both ductile and brittle deformation features (Schenker et al., 2014).

Foliation in the low-grade AVAZ imbricates is sub-parallel to the lithological contacts. It dips in general to the E, locally to the W due to a roll-over antiform close to the contact with the Pelagonian rocks (Fig. 5). Shear bands and SW-vergent drag folds indicate top-to-the-SW thrusting. Late and widely distributed top-to-the-E normal faults (Fig. 5) cut both the low-grade imbricates and the Cenomanian-to-Maastrichtian unconformable sediments.

The youngest, regionally distributed structures are E–W steep faults that bound to the west the Late Miocene–Pliocene Ptolemais-Kozani basins (Figs. 3 and 5, Koukouzas et al., 1979; Steenbrink et al., 2006). These normal faults displaced and placed lacustrine sediments at different elevations (Fig. 6). In 1995 an earthquake of magnitude 6.6 demonstrated recent activity of these faults (Pavlides et al., 1995).

1.2 Previously published low-temperature thermochronometric data

We present existing information in decreasing order of closure temperatures for mean cooling rates of 10 °C Ma^{-1} from 240 °C for ZFT, 180 °C for ZHe, 110 °C for AFT to 70 °C for AHe (e.g. Reiners and Brandon, 2006).

ZFT ages (Most et al., 2001; Most, 2003; Vamvaka et al., 2010) range between 86 and 61 Ma in the eastern part of north Pelagonia and span between 53 and 39 Ma in

the western part (Fig. 1b). To the south, they vary from 76 to 32 Ma (Most et al., 2001; Most, 2003; Vamvaka et al., 2010). Younger, 35–32 Ma old ZFT ages are located close to the Olympos window (Fig. 1b). In the AVAZ, ZFT ages are 80 Ma (Most, 2003). The western Rhodope yielded 72 Ma ZFT ages (Wüthrich, 2009).

ZHe in southern Pelagonia yields 53–36 Ma ages to the west and 30–20 Ma close to and within the Olympos window (Coutand et al., 2014). ZHe ages are younger, at 13 Ma to the south of the Olympos window (Fig. 1b). ZHe ages are not plotted for regional compilations (Fig. 1) since they are available in southern Pelagonia only and our data do not include ZHe ages. Nevertheless, they are implicitly taken into account as they have a similar age distribution as the ZFT ages.

AFT ages are 46 to 25 Ma in northern Pelagonia (Most et al., 2001; Most, 2003), 41 to 25 Ma in the southwest (Vamvaka et al., 2010; Coutand et al., 2014) and 18–11 Ma in the southeast (Most, 2003; Coutand et al., 2014). The few data in the AVAZ are 60–47 Ma (Most et al., 2001; Most, 2003). The western Rhodope yielded also AFT ages from 68 to 47 Ma (Kydonakis et al., 2014).

AHe ages in southern Pelagonia show a general eastward younging trend from 26 to 10 Ma (Coutand, 2014). This trend is associated with rapid cooling between 12 and 6 Ma around and in the Olympos window (Coutand et al., 2014).

Detrital apatites from Eocene-to-Miocene sediments of the southern Mesohellenic trough (Fig. 1b) show two age populations: at ca. 65 Ma and, more prominent, at ca. 40 Ma (Vamvaka et al., 2010).

2 New zircon and apatite fission-track dating

2.1 Method

The FT technique has been used to trace the low-temperature history of rocks collected along a SW–NE transect from both the footwall and hanging wall of major ductile shear zones to date fault activity and deformation from age differences between footwall and

hangingwall rocks (Figs. 3 and 5). Elevations of sampling sites were recorded (Table 1 and Fig. 5). FT ages were calculated with the ζ method (Hurford, 1990), ζ values are listed in Table 1.

Zircons and apatites were extracted with acoustic shockwaves produced in the SELFRAG apparatus (http://www.selfrag.com), ETH-Zürich. Standard heavy-liquid and magnetic separation delivered fractions enriched in apatite and zircon (Naeser, 1976). Zircon grains were mounted in teflon discs and apatites in epoxy. The mounts were polished to expose the internal surfaces of minerals and etched to visualize tracks. Zircons were etched for 25 to 28 h with NaOH-KOH in an eutectic melt at 220 °C. Apatites were etched for 20 s in 5.5 M HNO_3 at a controlled temperature of 21 °C. All samples were irradiated at the Oregon State University Reactor, along with low-U muscovite discs as external detectors, CN1 as fluence dosimeter for zircons or CN5 as fluence dosimeter for apatites, Durango and Fish Canyon Tuff standards. After irradiation, the external detectors were etched with 40 % HF for 45 min allowing visualization of the induced tracks.

2.2 Sample location and description

Sample location and details are given in Fig. 4 and Table 1.

2.2.1 Pelagonia

Samples 09-108, 09-120, 09-121, 09-055, 09-932, 09-098 and 10-090 are granitoids from the Pelagonian basement. These granitoids are characterized by variable gneissic textures from non-foliated to mylonitic and mineral assemblage attesting different metamorphic grades from amphibolite to greenschist facies. They generally contain quartz, plagioclase, biotite or chlorite, epidote, white mica, sphene, and horblende or actinolite.

2.2.2 AVAZ

Sample 10-029 from the AVAZ is a grain-supported conglomerate that belongs to the imbricated Upper Jurassic–Lower Cretaceous “Flysch-Phyllitic Series” (IGME, 1991). Clasts of Cr-spinel and hemicrystalline mafic fragments (likely of ophiolitic origin) suggest that these sediments were deposited in front of the AVAZ obduction. Chlorite blasts in sample 10-029 indicate low-grade metamorphism (Fig. 7a).

The samples 10-130 and 10-128 were collected in the upper beds of a ca. 350 m thick sedimentary sequence unconformably covering the AVAZ imbricates (Fig. 3). Sample 10–130 is a carbonatic matrix-supported conglomerate with pebbles of quartz, feldspar, serpentinites and schists. Sample 10–128 is a single, about 50 cm in diameter orthogneissic boulder from a clastic layer stratigraphic above sample 10-130. Sample 10-128 and 10-130 were not metamorphosed. The sedimentary sequence is characterized by marls intercalated with pebbly mudstones, carbonatic olistolites containing Late Cretaceous rudists (Appendix A) and conglomerates (Fig. 3) showing an up-sequence increase and coarsening of the detritus. The rudists are typical for the Pelagonian and AVAZ fauna attesting that the studied clastics were sourcing from these zones partially covered by carbonatic platforms and not from the Rhodope, where Rudists were not found (cf. Viquesnel, 1853; Sharp and Robertson, 2006). Marls covering unconformably the AVAZ thrust sheets contain the Turonian *Helvetoglobotruncana helvetica* (Figs. 3 and 7b), setting the lower deposition limit between 93.5 and 90 Ma (Bolli, 1945). The upper age limit of the stratigraphic column is < 66 Ma based on the Late Cretaceous *Globotruncana sp.* in marls (Figs. 3 and 7c).

2.3 Results

2.3.1 Zircon fission-track results

The pooled ZFT ages of the granitoids vary between 24 and 20.7 Ma (Fig. 1 and Table 1) with no discernible difference along the SW–NE transect. The results show no

relationship between age and elevation (Fig. 1 and Table 1). The χ^2-probability ($P(\chi^2)$) ranged between 18.5 and 95.8 %, which is well above the 5 % threshold of the $P(\chi^2)$-test; this indicates that each sample consists of a single age population (Galbraith, 1981).

The ZFT pooled ages in the sedimentary rocks yielded ages between 92.2 and 67.4 Ma (Table 1). ZFT ages in the low metamorphic-grade rock of sample 10-028 gave a single age population of 92.2 (−9 +10) Ma with a $P(\chi^2)$ value of 25.3 %. The age density histogram (Fig. 8a) exhibits a broad scatter of data from ca. 50 to 300 Ma. The sparse amount of countable zircons from this sample (n = 16, Table 1) prevented s g with statistical methods whether its ZFT ages are reset or detrital. Nevertheless, the metamorphic growth of chlorite indicates peak temperatures above 250 °C (Spear, 1995) that have partially or totally reset the zircons at 92.2 (+10 −9) Ma. The gneissic boulder (10-128) in the Upper Cretaceous sedimentary unit yielded a single age population at 67.4 (−4.8 +5.2) Ma $P(\chi^2)$ 15 % (Fig. 4 and 5 and Table 1). The unmetamorphosed ks of sample 10-130 showed a pooled age of 76.2 (−5.7 +6.2) Ma with a $P(\chi^2)$ value of 1.7 % indicating that the age distribution consists of multiple populations. Using the Binomfit computer program (Brandon, 1996), two populations were estimated: (i) a Late Cretaceous one at 68 (−6.1 +5.6) Ma and (ii) a Late Jurassic one at 179.6 (−56 +42.8) Ma (Fig. 8b).

2.3.2 Apatite fission-track results

The basement AFT ages are distributed between 22.9 and 16.1 Ma. As the ZFT ages, these ages show no correlation with elevation and no discernible difference along the profile (Fig. 5 and Table 1). Only the easternmost sample (10-090, Figs. 4 and 5, pooled age = 22.9 Ma) is significantly older than the others: its upper 68 % confidence interval is 1.3 Ma older that the lower 68 % confidence interval of the closest sample to the west (09-098, pooled age = 16.1 Ma). The $P(\chi^2)$ values of the granitoid AFT cooling ages were between 2.8 and 99.6 %. Exceptionally for magmatic rocks, sample 09-055

failed the χ^2-test ($P(\chi^2)$ = 2.8 %). The grain age distribution of this sample was strongly affected by one grain with an old age (46.1 Ma) (Fig. 9). The omission of this outlier-grain resulted in a $P(\chi^2)$ value of 17 % without affecting significantly either the central or the pooled age, which remain unchanged within error (17.6, −1.4 +1.5 Ma). Moreover, apatites of sample 09-055 showed high spread of U-concentration with values up to 126 ppm and D_{par} values ranging between 1.5 and 2.2 µm (Fig. 9). The D_{par} is the arithmetic mean maximum diameter of FT etch-figures, and this parameter is used to infer the relative resistance to annealing (Burtner et al., 1994; Carlson et al., 1999). The relative wide range of D_{par} values of sample 09-055 could partly explain the spread of its grain ages resulting in a low $P(\chi^2)$ value. The large age distribution of this sample may also be due ts high spread of U-concentration that causes significant radiation damage of apatites. Although no experimental data exist on the influence of radiation damage on the FT annealing kinetics in apatites, it is commonly argued that it may play a role (Carlson et al., 1999). Because both the D_{par} and U-concentration values of this samples hint to compositional heterogeneity, and because the ZFT age of this sample is consistent with a single population centered at 23.1 Ma, we conclude that its AFT age distribution reflects variable annealing resistance and does not relate to partial-resetting conditions.

The only AFT age from the Vardar unit (10-128) is 32.7 (+3.4 −3.1) Ma with a $P(\chi^2)$ value of 13.7 %. As discussed in the previous paragraph, sample 10-128 is a gneissic boulder in the unmetamorphosed sediments containing Upper Cretaceous *Globotruncana* (Figs. 3 and 7c). Therefore, young apatites in the ca. 66 Ma sediments have been totally reset at ca. 33 Ma or earlier, and they cooled below 110 °C (AFT closure temperature) at 32.7 Ma. The ZFT age of this sample was not reset which implies that temperatures that have reset apatite did not rise beyond 220–240 °C.

2.3.3 Inverse modeling of fission-track lengths and estimate of closure temperatures

Thermal history reconstructions were performed using inverse modeling of the AFT lengths with the HeFTy computer program (Ketcham, 2005) according to the annealing model of (Ketcham et al., 2007). Due to the high U-content of its apatites (Fig. 9), sample 09-055 was the only one that showed enough horizontal confined tracks (54) for statistical validity. As discussed in Sect. 3.2, these apatite grains have a complex annealing behavior. Taking into account this complexity, we performed several models, which all resulted in a consistent thermal history exemplified by the model shown in Fig. 10. This model represents the simplest case of a single-age population. The t-T-paths were forced to cross two fields (Fig. 10a): (i) from 20 to 26.6 Ma (95 % confidence interval (CI) from ZFT ages of the same sample) in the temperature window between 260 and 220 °C as defined by the closing temperature of zircons (e.g. Reiners and Brandon, 2006), (ii) from 7 to 3 Ma ~~(the time of exposure of the Pelagonian basement at surface temperature~~) between 30 to 0 °C as defined by unconformable coal and lacustrine sediments (Steenbrink et al., 2006) containing gastropods (art *Radix Auriculata*, Fig. 7d) not older than Pliocene (Fig. 10c).

HeFTy calculated an AFT age of 19.5 (+3.1 −2.7) Ma and a mean track length of 12.59±2.33 µm for sample 09-055 (Fig. 10a and b). The best-fit model gave a goodness of fit index (GOF) of 0.96 for the model age, and of 0.97 for the track lengths (Fig. 10a). The inverse modeling of the track lengths resulted in three-steps cooling history (Fig. 10), from which we can roughly estimate cooling rates of: (i) 20–40 °C Ma^{-1} between 27 and 21 Ma, (ii) 1–3 °C Ma^{-1} from 21 to 7 Ma; and (iii) from below 80 °C to surface temperatures in 2–4 Ma between 7 to 3 Ma.

3 Discussion

3.1 Detrital fission-track ages of the western AVAZ: 68 Ma abrupt and fast denudation of Pelagonia

In the studied area, the low-grade AVAZ imbricates (sample 10-029) have been covered unconformably by marine sediments between 93.5 and 90 Ma. The ZFT cooling age of these imbricates at 92.2 Ma has a large uncertainty (−9 +10 Ma) that overlaps with the age of the unconformity. As a consequence, cooling below ca. 240 °C is placed between 102 Ma, which is the upper 68 % confidence interval of the ZFT age of sample 10-029, and 93.5–90 Ma, which is the erosional unconformity.

On the regional scale, marine conditions were installed over the Pelagonian and the AVAZ until 66 Ma, starting from an unconformity variable in space and time between the Cenomanian and the Early Aptian (100–80 Ma). Deepening of the basin corresponds to a long history of residence at temperatures < 240 °C between 86 and ca. 68 Ma in northern Pelagonian basement, at 80 Ma in the eastern AVAZ and at 7[illegible]a in western Rhodope (Fig. 1b). This shows post-collisional cooling and thermal subsidence of the external orogenic pile throughout the late [illegible]aceous (Fig. 11a).

The increase of detritus at ca. 66 Ma (Fig. 3) marks the end of the 20–30 Ma long period of regional cooling and sedimentation. The ZFT age at 68 (−6.1 +5.6) Ma (youngest detrital population of sample 10-130) and at 67.4 (−4.8 +5.2) Ma (gneissic boulder of sample 10-128), overlaps the depositional age within error. The short lag time between cooling, erosion and deposition indicates fast denudation. The clastic sediments are very coarse, suggesting short transport distances and mechanical erosion. The gneissic clasts and the rudists-bearing olistolites constrain the sediment catchment to be in the now eroded southeastern Pelagonia, which has a similar cooling age as northern Pelagonia (Fig. 11b). Abrupt and rapid cooling at ca. 68 Ma occurred during thrust migration that first buried the ca. 70 Ma syn-orogenic mass flows of the AVAZ (Mercier and Vergely, 1994) and then the 40–38 Ma External Hellenides (Brunn, 1956; Ferriére et al., 2004). Thrusting was accompanied by blueschist metamorphism

dated between 61 and 42 Ma with Ar/Ar on white micas (Fig. 11b, Schermer et al., 1990). During the thermal overprint and relaxation of this compressional event, western Pelagonia cooled below 240 and 110 °C throughout the Eocene (Fig. 11b and c).

3.2 Cooling and exhumation of the central-eastern Pelagonian basement: late Oligocene-to-Miocene extension

New ZFT and AFT ages indicate Late Oligocene–Early Miocene cooling of the crystalline rocks of central-eastern Pelagonia. The small age difference between ZFT and AFT data (locally the 65 % confidence interval overlaps), and inverse modeling of the track lengths suggest fast and spatially uniform cooling from ca. 240 to ca. 80 °C between 24 and 21 Ma. In the absence of Late Oligocene–Early Miocene advected heat source (Schenker et al., 2014), this fast cooling hints to tectonic denudation along the reactivated top-to-the E–NE shear zone at the eastern margin of the Pelagonia (Figs. 5 and 11d). This normal shear zone now separates ca. 68 Ma detrital ZFT and 32.7 Ma reset AFT ages in the hanging wall from 24–20.7 Ma ZFT and 22.9–16.9 Ma AFT ages in the footwall (Fig. 5). In the hanging wall, extensional tectonic slices (Fig. 11c and d) incorporate the reset 32.7 (−3.1 +3.4 Ma) AFT age of sedimentary sample 10-128. This suggests that extension in the AVAZ started even earlier, at ca. 33 Ma.

Two mechanisms are envisaged for the 33–16 Ma extension in central-eastern Pelagonia: (i) local extension above an antiformal stack duplex during continuous underthrusting of the External Hellenides (Ferriére et al., 2004), (ii) distributed extension during southward rollback of the Hellenic slab (e.g. Le Pichon et al., 1979; Brun and Faccenna, 2008) after the Eocene–Oligocene compression. At ca. 15 Ma the trench of the Hellenic subduction was already migrating westward over 80 km and was located at ca. 200 km from the central-eastern Pelagonia (Royden and Papanikolaou, 2011). Assuming a slab with low angle (30°) at this time, the slab interface was at ca. 115 km below central-eastern Pelagonia. Because a duplex of 115 km is mechanically unrealistic, hypothesis (i) is discarded. Therefore, the 33–16 Ma cooling is the oldest

and north-easternmost thermal expression of the southward rollback of the Hellenic slab.

3.3 Pliocene cooling and uplift

During the Late Miocene–Pliocene lacustrine sediments locally covered the Pelagonian basement of the studied area attesting exposure after 7 Ma. These data have been used to constrain the inverse modeling of the FT lengths, which discloses rapid cooling after ca. 7 Ma from the upper AFT partial retention zone at ca. 80 °C to the surface. E–W normal faults cutting the lacustrine sediments demonstrate recent extension (Figs. 3, 4, and 10c). Footwalls of these faults uplifted the lacustrine sediments more than 500 m and were carved by rivers in a concave-up shape typical for active uplifting (Fig. 6). Therefore, the conspicuous relief in the central Pelagonia was built after 7 Ma ~~(Fig. 11e)~~. These E–W faults have been interpreted as sinistral strike-slips with horizontal displacement of ca. 20 km (van Hinsbergen and Schmid, 2012) because they are coeval and parallel to the sinistral North Anatolia fault (Fig. 11e). Nevertheless, our geological map and direct observations of fault ~~striations~~ contradict any significant strike slip movement (Fig. 4). Furthermore, the large distribution of normal faults over 50 km graving the intra-montane basins of Kosani and Ptolemais (Fig. 11e) tangibly attests regional N–S extension rather than inferred, localized strike slip faulting.

4 Conclusions

Several compressive and extensive events occurred from the Mesozoic to the Cenozoic in the Pelagonian and the adjacent AVAZ. Their late thermal effects and extent were constrained with ZFT and AFT ages recording protracted cooling events as follows (Fig. 11):

i. *Cooling below 240 °C of the metamorphic western AVAZ imbricates between 102 and 93–90 Ma, of northern Pelagonia between 86 and 68 Ma, of the eastern*

AVAZ at 80 Ma and of western Rhodope at 72 Ma. The 30–20 Ma-long and heterogeneous regional cooling is contemporaneous with subsidence of Late Cretaceous marine basin(s) covering since 100 Ma the external zones of the nappe pile formed at 130–110 Ma.

ii. *Abrupt and rapid cooling below 240°C of the Pelagonian basement at about 68 Ma* due to erosional denudation during thickening. Its thermal effect lasted until ca. 40 Ma according to ZFT and AFT in western and eastern Pelagonia, respectively (cf. Fig. 11b).

iii. *Cooling below 120°C of the western AVAZ from 33 Ma and between 240 and 80°C of the central-eastern Pelagonian basement from 24 to 16 Ma*. These two zones cooled from different tectonic levels in the footwall of westward migrating normal faults with top-to-the-NE sense of shear (Fig. 11c and d). Extension is attributed to rollback of the Hellenic slab.

iv. *post-7 Ma cooling below 80°C* during Pliocene-to-recent, normal faulting in central-eastern Pelagonia (Fig. 11e).

The complex low-temperature history of the Pelagonian basement and the AVAZ preserved the record of a long residence at temperature below 240 °C from 102 Ma onwards. Thus, since that time these tectonic units have not been involved in major crustal-scale burial processes invoking elevated thermal condition. In this upper-crustal tectonic context, the combined use of fission-track dating, structural and stratigraphic data was essential to unravel polyphase tectonic processes extending over a long time-interval.

Appendix A: Description of Rudist in olistolites of the Upper Cretaceous sedimentary sequence

Lenticular or blocky olistolites of recrystallized limestone contain Rudist, Oyster, Corals and benthic Foraminifera. Three Rudists show a post-Cenomanian to Maastrichtian genus: (i) *Durania* (*Radiolitid*), (ii) *Radiolitidae* and (iii) *Plagioptychid*. Although none of these generic identifications can yet be considered secure without closer study, the Rudists show independently the same lower stratigraphic boundary. This fixes the existence of a carbonatic platform in the Mid-Late-Cretaceous.

i. *Durania (Radiolitid)*

A shell fragment shows a multi-layered structure with a dark inner and a complex outer layer. This outer layer has a ca. 1 cm thick cellular structure in the internal part and a 3 mm thick lenticular structure in the external part (Fig. A1a). The outer lenticular structures are the expression, in transverse section, of fine regular riblets on the surface of the shell, in this case adjoining those from a superficial fragment of another shell, which probably was attached to it. The cellular texture of the outer layer and the regular fine external riblets characterize a fragment of *Durania* (*Radiolitid*) (e.g. Cobban et al., 1991). In order to confirm this generic identification, however, we would need to observe the absence of a ligamentary infolding on the dorsal inner margin of the outer shell layer, as well as distinct radial bands with finer ribbing on its external posteroventral flank; unfortunately, none of these parts of the shell is visible in this fragment. The most abundant occurrence of *Durania* is in the Upper Albian to the Maastrichtian, even without a regular outer layer (like the shell in Fig. A1a), which is not typical for the Upper Cretaceous Genus. This specimen is probably not older than Cenomanian (e.g. Cobban et al., 1991).

ii. *Radiolitidae* with prominent ornaments in the outer layer

The shells consist of an internal thin layer and an external polygonal mesh, representing a traverse section through a Rudist valve (Fig. A1b). The regular polygonal (mostly hexagonal) shell ornament of the outer layer is characteristic

for rudists of the family *Radiolitidae*. The first representative, with a poorly developed cellular layer, is Albian (Fenerci-Masse et al., 2006). The more prominent celluloprismatic outer layer (as in Fig. A1b) is typically well developed in the Cenomanian up to the Maastrichtian forms (e.g. Fenerci-Masse et al., 2006).

iii. *Plagioptychid*

The outer valve layer displays radial lines that are interpreted as pallial canals separated by tightly bifurcating laminae. Valve inwards, there is a 1 mm white calcitic layer with no discernible internal textures, followed by a 3 mm grey layer and a 2 mm lighter layer with no discernible internal textures (Fig. A1c and d). The grey layer is probably constituted by detrital components, hinting to cavity fill in the inner-valve layer (the latter consists of the two calcitic layers with no internal structure). The form of the canals and the cavity in the internal layer are typical for the left valve of *plagioptychids* (Fig. 7 of Skelton, 2013). The *plagioptychids* range from the upper Turonian to the Maastrichtian (e.g. Skelton, 2013).

Acknowledgements. We thank the following people for help with fossil identification: P. Hochueli (gastropod), D. Bernoulli and S. Spezzaferri (foraminifera), P. Skelton and I. Stössel (rudists).

References

Anders, B., Reischmann, T., and Kostopoulos, D.: Zircon geochronology of basement rocks from the Pelagonian Zone, Greece: constraints on the pre-Alpine evolution of the westernmost Internal Hellenides, Int. J. Earth Sci., 96, 639–661, 2007.

Bernoulli, D. and Laubscher, H.: The palinspastic problem of the Hellenides, Eclogae Geol. Helv., 65, 1007–1118, 1972.

Bolli, H.: Zur Stratigraphie der Oberen Kreide in den höheren helvetischen Decken, Eclogae Geol. Helv., 37, 226–227, 1945.

Bonneau, M., Godfriaux, I., Moulas, Y., Fourcade, E., and Masse, J.: Stratigraphie et structure de la bordure orientale de la double Fenêtre du Païkon (Macédoine, Grèce), Bull. Geol. Soc. Greece, XXX/1, 105–114, 1994.

Brandon, M. T.: Probability density plot for fission-track grain-age samples, Radiat. Meas., 26, 663–676, 1996.

Brun, J. P. and Faccenna, C.: Exhumation of high-pressure rocks driven by slab rollback, Earth Planet Sc. Lett., 272, 1–7, 2008.

Brunn, J.: Contribution à l'étude Géologique du Pinde septentrional et d'une partie de la Macédoine Occidentale, Ann. Geol. Pays. Hellen., 7, 1–358, 1956.

Burg, J.-P.: Rhodope: from Mesozoic convergence to Cenozoic extension. Review of petro-structural data in the geochronological frame, Journal of the Virtual Explorer, 42, 44 pp., 2012.

Burtner, R. L., Nigrini, A., and Donelick, R. A.: Thermochronology of lower Cretaceous source rocks in the Idaho-Wyoming thrust belt, AAPG Bulletin-American Association of Petroleum Geologists, 78, 1613–1636, 1994.

Carlson, W. D., Donelick, R. A., and Ketcham, R. A.: Variability of apatite fission-track annealing kinetics: I. Experimental results, Am. Mineral., 84, 1213–1223, 1999.

Cobban, W., Skelton, P., and Kennedy, W.: Occurrence of the rudistid Durania cornupastoris (Des Moulins, 1826) in the Upper Cretaceous Greenhorn Limestone in Colorado, US Geological Survey Bulletin for 1985, D1–D8, 1991.

Coutand, I., Walsh, M., Louis, B., Chanier, F., Ferriére, J., and Reynaud, J.-Y.: Neogene Upper-Crustal Cooling of the Olympus Range (Northern Aegean): Major Role of Hellenic Back-Arc Extension Over Propagation of the North Anatolia Fault Zone, Terra Nova, 2014.

Fenerci-Masse, M., Massr, J. P., Arias, C., and Vilas, L.: Archaeoradiolites, a new genus from the Upper Aptian of the Mediterranean region and the origin of the rudist family Radiolitidae, Palaeontology, 49, 769–794, 2006.

Ferriére, J., Reynaud, J.-Y., Pavlopoulos, A., Bonneau, M., Migiros, G., Chanier, F., Proust, J.-N., and Gardin, S.: Geologic evolution and geodynamic controls of the Tertiary intramontane piggyback Meso-Hellenic basin, Greece, Bull. Soc. Géol. Fr., 175, 361–381, 2004.

Galbraith, R. F.: On statistical models for fission track counts, Math. Geol., 13, 471–477, 1981.

Godfriaux, I., Ferriere, J., and Schmitt, A.: Le développement en contexte continental d'un métamorphisme HP/BT: les "schistes bleus" tertiaires Thessaliens, Bullet. Geol. Soc. Greece, XXX/1, 175–192, 1988.

Hurford, A. J.: International-Union-of-Geological-Sciences subcommission on geochronology recommendation for the standardization of fission-track dating calibration and data reporting, Nucl. Tracks Rad. Meas., 17, 233–236, 1990.

IGME: Kolindros Sheet, Geological Map of Greece 1 : 50 000, Institute of Geology and Mineral Exploration, Greece, 1991.
Ivanova, D., Bonev, N., and Chatalov, A: Biostratigraphy and tectonic significance of lowermost Cretaceous carbonate rocks of the Circum-Rhodope Belt (Chalkidhiki Peninsula and Thrace region, NE Greece), Cretac. Res., 52, 25–63, 2015.
Jacobshagen, V., Dürr, S., Kockel, F., Kopp, K. O., Kowalczyk, G., Berckhemer, H., and Büttner, D.: Structure and geodynamic evolution of the Aegean region, in: Alps, Appenines, Hellenides, edited by: Cloos, H., Roeder, D., and Schmidt, K., E. Schweizerbart'sche Verlagsbuchhandlung, Stuttgart, 537–564, 1978.
Ketcham, R. A.: Forward and inverse modeling of low-temperature thermochronometry data, Rev. Mineral. Geochem., 58, 275–314, 2005.
Ketcham, R. A., Carter, A., Donelick, R. A., Barbarand, J., and Hurford, A. J.: Improved modeling of fission-track annealing in apatite, Am. Mineral., 92, 799–810, 2007.
Kilias, A., Frisch, W., Avgerinas, A., Dunkl, I., Falalakis, G., and Gawlick, H. J.: Alpine architecture and kinematics of deformation of the northern Pelagonian Nappe Pile in the Hellenides, Austr. J. Earth Sci., 103, 4–28, 2010.
Koukouzas, C. N., Kotis, T., Ploumidis, M., and Metaxas, A.: Coal Exploration of Anargiri Area, Amynteon (W. Macedonia), Mineral Deposit Research, Natl. Instit. Geol. Mining Res., 5–14, 22–34, 1979.
Kydonakis, K., Gallagher, K., Brun, J. P., Jolivet, M., Gueydan, F., and Kostopoulos, D.: Upper Cretaceous exhumation of the western Rhodope Metamorphic Province (Chalkidiki Peninsula, northern Greece), Tectonics, 33, 1–20, 2014.
Le Pichon, X., Angelier, J., Aubouin, J., Lyberis, N., Monti, S., Renard, V., Got, H., Hsu, K., Mart, Y., Mascle, J., Matthews, D., Mitropoulos, D., Tsoflias, P., and Chronis, G.: From subduction to transform motion – seabeam survey of the Hellenic trench system, Earth Planet Sc. Lett., 44, 441–450, 1979.
Lecassin, R., Arnaud, N., Leloup, P. H., Armijo, R., and Meyer, B.: Syn- and post-orogenic exhumation of metamorphic rocks in North Aegean, eEarth, 2, 51–63, 2007.
Lock, J. and Willett, S.: Low-temperature thermochronometric ages in fold-and-thrust belts, Tectonophysics, 456, 147–162, 2008.
Mavridou, E., Antoniadis, P., Khanaqa, P., Riegel, W., and Gentzis, T.: Paleoenvironmental interpretation of the Amynteon-Ptolemaida lignite deposit in northern Greece based on its petrographic composition, Int. J. Coal Geol., 56, 253–268, 2003.

Mercier, J. and Vergely, P.: Is the Païkon Massif a tectonic window in the Axios-Vadar zone? (Internal Hellenides, Macedonia, Greece), Bull. Geol. Soc. Greece, XXX/1, 115–120, 1994.
Most, T.: Geodynamic evolution of the Eastern Pelagonia zone in the Northwestern Greece and the Republic of Macedonia, Geowissenschaftlichen Fakultät, Eberhardt-Karls-Universität Tübingen, Tübingen, 195 pp., 2003.
Most, T., Frisch, W., Dunkl, I., Kadosa, B., Boev, B., Avgerinas, A., Kilias, A.: Geochronological and structural investigations of the northern Pelagonian crystalline zone – constraints from K/Ar and zircon and apatite fission track dating, Geol. Soc. Greece Bull., 34, 91–95, 2001.
Naeser, C. W.: Fission-track dating, in: US Geological Survey Open File Report, 76–190, 1976.
Papanikolaou, D.: The tectonostratigraphic terranes of the Hellenides, Annales Géologiques des Pays Helléniques, 37, 495–514, 1997.
Papanikolaou, D.: Timing of tectonic emplacement of the ophiolites and terrane paleogeography in the Hellenides, Lithos, 108, 262–280, 2009.
Pavlides, S. B., Zouros, N. C., Chatzipetros, A. A., Kostopoulos, D. S., and Mountrakis, D. M.: The 13 May 1995 Western Macedonia, Greece (Kozani-Grevena) earthquake – preliminary-results, Terra Nova, 7, 544–549, 1995.
Reiners, P. W. and Brandon, M. T.: Using thermochronology to understand orogenic erosion, Annu. Rev. Earth Pl. Sc., 34, 419–466, 2006.
Renz, C. and Reichel, M.: Beiträge zur Stratigraphie und Paläontologie des Ostmediterranen Jungpaläozoikums und dessen Einordnung im griechischen Gebirgsystem, Eclogae Geol. Helv., 38, 221–313, 1945.
Royden, L. H., Papanikolaou, D. J.: Slab segmentation and late Cenozoic disruption of the Hellenic arc, Geochem. Geophy. Geosy., 12, doi:10.1029/2010GC003280, 2011.
Schenker, F. L., Burg, J.-P., Kostopoulos, D., Moulas, E., Larionov, A., and von Quadt, A.: From Mesoproterozoic magmatism to collisional Cretaceous anatexis: tectonomagmatic history of the Pelagonian Zone, Greece, Tectonics, 1552–1576, 2014.
Schermer, E. R.: Geometry and kinematics of continental basement deformation during the Alpine orogeny, Mt. Olympus region, Greece, J. Struct. Geol., 15, 571–591, 1993.
Schermer, E. R., Lux, D. R., and Burchfiel, B. C.: Temperature–time history of subducted continental-crust, Mount Olympos Region, Greece, Tectonics, 9, 1165–1195, 1990.
Sharp, I. R. and Robertson, A. H. F.: Tectonicsedimentary evolution of the western margin of the Mesozoic Vardar Ocean: evidence from the Pelagonian and Almopias zones,

northern Greece, in: Tectonic Development of the Eastern Mediterranean Region, edited by: Robertson, A. H. F., and Mountrakis, D., Geological Society, London, 373–412, 2006.
Skelton, P. W.: Rudist classification for the revised Bivalvia volumes of the "Treatise on Invertebrate Paleontology", Caribb. J. Earth Sci., 45, 9–33, 2013.
Spear, F. S.: Metamorphic Phase Equilibria and Pressure–Temperature–Time Paths, Washington, DC, 1995.
Steenbrink, J., Hilgen, F. J., Krijgsman, W., Wijbrans, J. R., and Meulenkamp, J. E.: Late Miocene to Early Pliocene depositional history of the intramontane Florina-Ptolemais-Servia Basin, NW Greece: Interplay between orbital forcing and tectonics, Palaeogeogr. Palaeocl., 238, 151–178, 2006.
Vamvaka, A., Spiegel, C., Frisch, W., Danisik, M., and Kilias, A.: Fission track data from the Mesohellenic Trough and the Pelagonian zone in NW Greece: cenozoic tectonics and exhumation of source areas, Int. Geol. Rev., 52, 223–248, 2010.
van Hinsbergen, D. J. J. and Schmid, S. M.: Map view restoration of Aegean-West Anatolian accretion and extension since the Eocene, Tectonics, 31, doi:10.1029/2012TC003132, 2012.
Viquesnel, A.: Résumé des observations géographiques et géologiques faites, en 1847, dans la Turquie d'Europe, Bull. Soc. Géol. Fr., 2, 454–475, 1853.
Wüthrich, E. D.: Low Temperature Thermochronology of the Northern Aegean Rhodope Massif, Earth Sciences, Swiss Federal Institute of Technology Zurich, Zurich, 210 pp., 2009.
Yarwood, G. A. and Dixon, J. E.: Lower Cretaceous and younger thrusting in the Pelagonian rocks of High Piera, Greece, in: 6th Colloq. Aegean Region, Athens, 1, 269–280, 1977.

Table 1. Pooled ages calculated using dosimeter glass CN5 and CN1 for zircons and apatites, respectively. ρ_s, spontaneous track densities measured in internal mineral surfaces; N_s, total number of spontaneous tracks; ρ_i and ρ_d induced and dosimenter track densities on external mica detectors; N_i and N_d total numbers of tracks; $P(\chi^2)$, probability of obtaining χ^2 value for y degrees of freedom (where y = number of crystals −1).

sample	unit/rock type	coordinates	elevation [m]	No. of grains	ρ_d [tracks cm^{-2}]	ρ_s [tracks cm^{-2}]	N_s	ρ_i [tracks cm^{-2}]	N_i	$P(\chi^2)$ [%]	pooled age 68 % CI [Ma]	-2σ	$+2\sigma$	local ζ-CN
zircon FT age														
09-032	Pelagonian basement/leucogneiss	N40°23′45.4″ E022°06′18.5″	1330	20	3.51E+05	6.14E+06	581	6.39E+06	605	25.4	24	1.7	1.9	142.57 ± 5.95
09-055	Pelagonian basement/granodiorite	N40°19′11.6″ E022°05′53.8″	320	20	3.33E+05	8.05E+06	666	8.27E+06	684	18.5	23.1	1.6	1.7	142.57 ± 5.95
09-098	Pelagonian basement/leucogneiss	N40°21′21.4″ E022°09′39.5″	250	20	3.36E+05	4.75E+06	429	4.72E+06	427	95.8	24	1.9	2.1	142.57 ± 5.95
09-108	Pelagonian basement/granodioritic gneiss	N40°19′50.6″ E022°03′19.4″	1020	20	3.45E+05	5.08E+06	479	6.02E+06	568	61.6	20.7	1.5	1.7	142.57 ± 5.96
10-029	AVAZ/late Upper Jurassic–Cretaceous conglomerate	N40°26′10.8″ E022°16′00.7″	760	16	4.56E+05	7.90E+06	447	2.76E+06	156	25.3	92.2	9	10	142.57 ± 5.95
10-128	AVAZ/gneissic block in Upper Cretaceous conglomerate	N40°27′45.1″ E022°12′26.7″	530	21	4.55E+05	9.22E+06	901	4.41E+06	431	15	67.4	4.8	5.2	142.57 ± 5.95
10-130	AVAZ/Upper Cretaceous conglomerate	N40°27′37.6″ E022°13′10.4″	440	27	4.59E+05	4.52E+06	881	1.93E+06	376	1.7	76.2	5.7	6.2	142.57 ± 5.96
apatite FT ages														
09-055	Pelagonian basement/granodioritic gneiss	N40°19′11.6″ E022°05′53.8″	320	27	1.37E+06	5.60E+05	326	6.59E+06	3838	2.8	19.5	1.4	1.5	335.93 ± 14.96
09-098	Pelagonian basement/leucogneiss	N40°21′21.4″ E022°09′39.5″	240	38	1.34E+06	8.84E+04	48	1.24E+06	673	99.6	16.1	2.4	2.7	335.93 ± 14.96
09-108	Pelagonian basement/granodioritic gneiss	N40°19′50.6″ E022°03′19.4″	1020	24	1.47E+06	1.83E+05	69	2.57E+06	971	66.4	17.6	2.2	2.5	335.93 ± 14.96
09-120	Pelagonian basement/leucogneiss	N40°16′43.3″ E022°06′50.8″	1000	23	1.42E+06	2.67E+05	73	3.46E+06	947	94.5	18.5	2.2	2.6	335.93 ± 14.96
09-121b	Pelagonian basement/granodioritic gneiss	N40°13′37.0″ E022°06′34.4″	1200	25	1.31E+06	5.23E+05	131	6.30E+06	1577	68.9	18.5	1.7	1.9	339.54 ± 12.53
10-090	Pelagonian basement/granodioritic gneiss	N40°24′15.3″ E022°11′33.6″	160	25	1.23E+06	2.21E+05	69	2.03E+06	633	23.2	22.9	2.8	3.2	339.54 ± 12.53
10-128	AVAZ/gneissic block in Upper Cretaceous conglomerate	N40°27′45.1″ E022°12′26.7″	530	20	1.60E+06	3.76E+05	131	3.13E+06	1091	13.7	32.7	3.1	3.4	339.54 ± 12.53

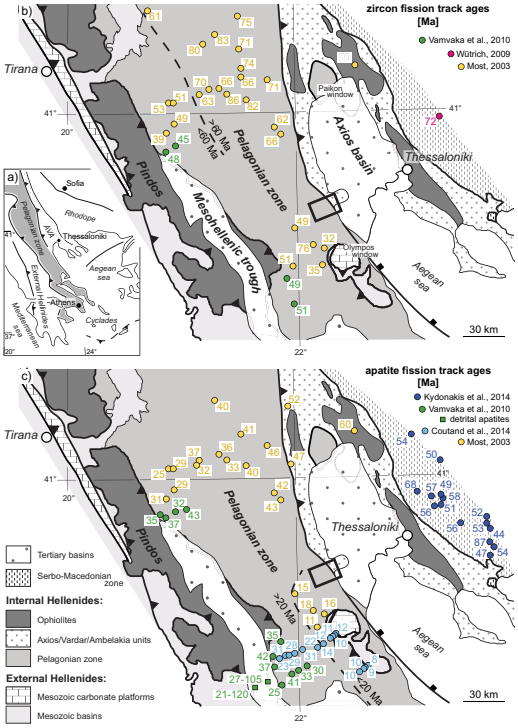

Figure 1. ~~(a)~~ overview map ~~(centre left)~~ and tectonic maps of the Helle s (modified after Burg, 2012) with publishes ZFT ages **(b)** and AFT ages **(c)**. Errors of the FT ages between 1.6 and 11 Ma. Detrital AFT data are reported as the range of single-grain ages. In the southern Pelagonia, ZHe and AHe ages of Countand (2014) ar to, respectively, ZFT and AFT ages pattern. Working area shown in the black frame.

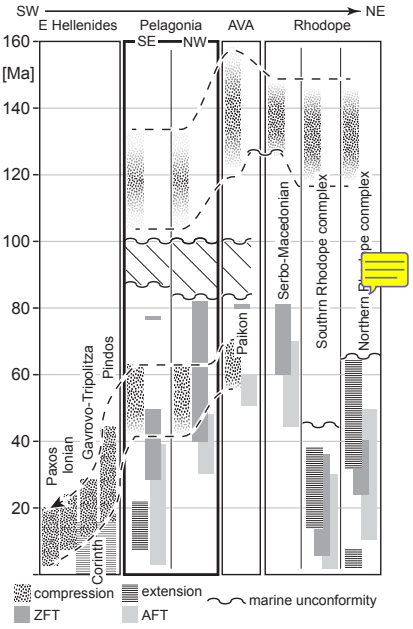

Figure 2. Compilation of zircon and apatite FT ages (references in Fig. 1) with main tectonic events. From southwest to northeast: tectonism of Paxos, Ionian, Gavrovo-Tripolitza and Pindos (= typical localities of the first deposition of the syn-orogenic mass flow deposits) according to Papanikolaou (1997); Pelagonia unconformity and tectonic according to Kilias et al. (2010); Schenker et al. (2014), respectively; Paikon (= Late Cretaceous/Early Tertiary window in the AVAZ) tectonism according to ~~Bonneau~~ et al. (1994); Mercier and Vergely (1994); tectonism and transgressions of Serbo-Macedonian (= the westernmost continental fragment of the Rhodope) and Southern and Northern Rhodope Complexes (= two extensional metamorphic core complexes) according to Burg (2012) and Ivanova et al. (2015).

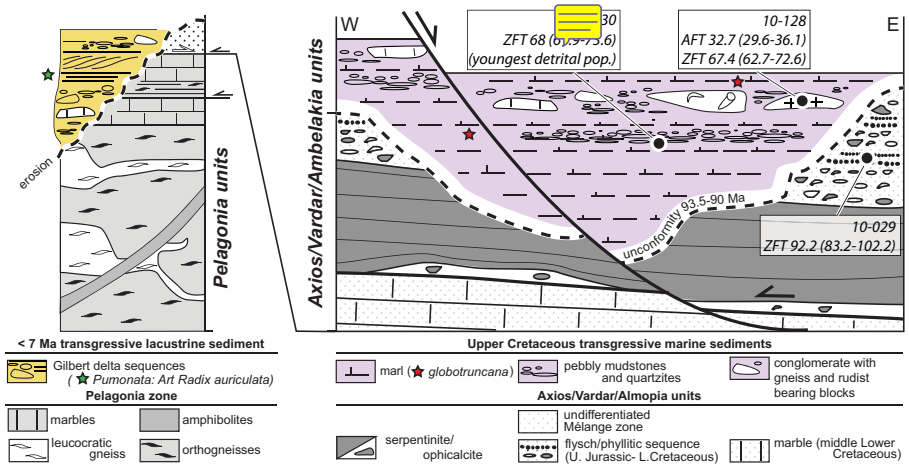

Figure 3. Tectono-stratigraphic column of the Pelagonian zone and schematic field relationships of the AVAZ with sample location and FT ages. FT ages shown with 2σ confidence interval. The displacement of the normal fault in the AVAZ is unknown.

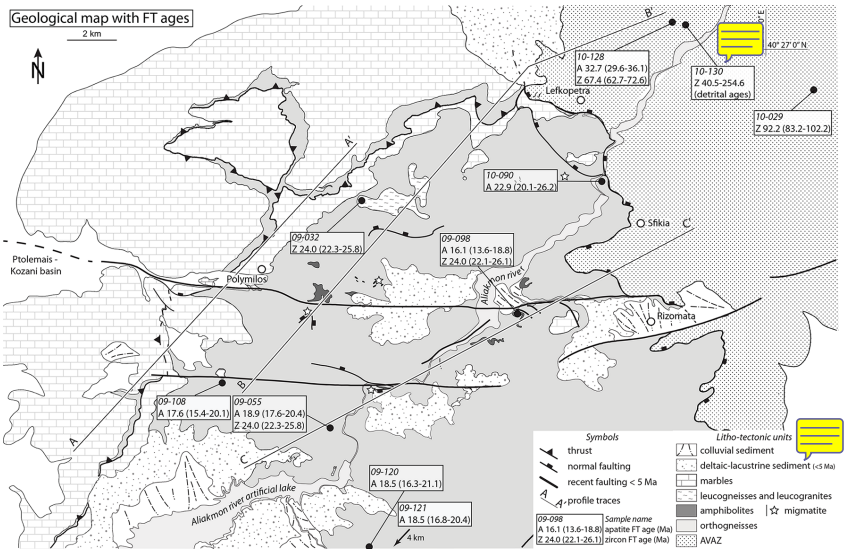

Figure 4. Location and age of FT samples (pooled age and the 68 % confidence interval) on the geological map (located in Fig. 1) of the eastern Pelagonian gneiss dome Schenker (2014). For the detrital zircons of sample 10-130, the range of single-grain ages is reported.

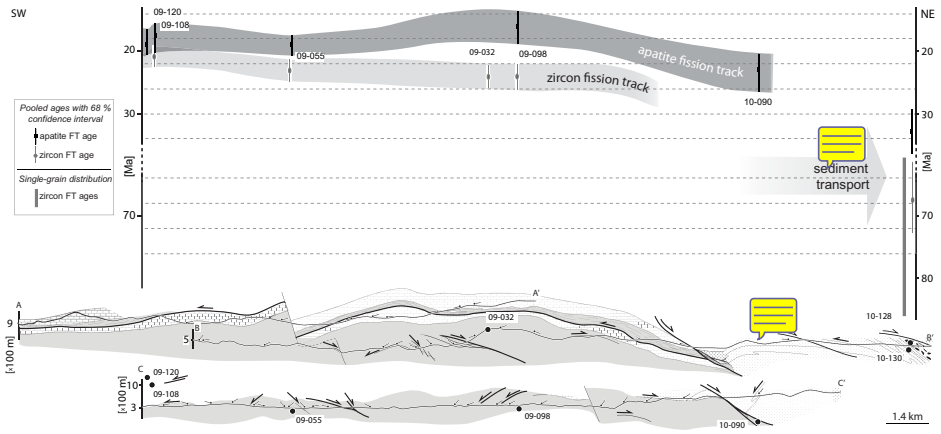

Figure 5. AFT and ZFT ages along three transects across the eastern Pelagonia gneiss dome. For the location of the transects see Fig. 2.

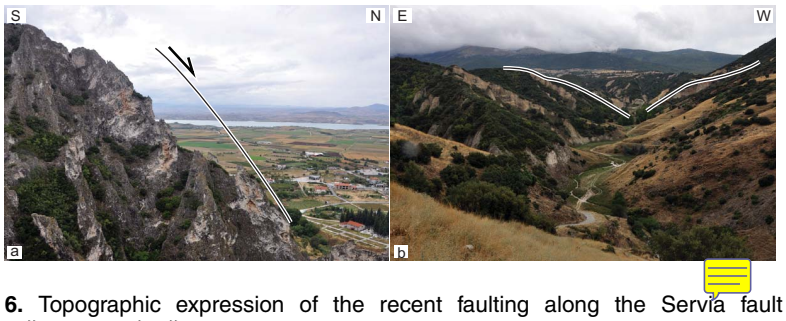

Figure 6. Topographic expression of the recent faulting along the Servia fault (GPS: N40°10′37″, E021°59′50″). **(a)** Erosion features on the fault scarp. On the horizon the Kozani plane (elevation ca. 280 m) filled with Pliocene to recent lacustrine sediments which are found at elevations of ca. 800 m in the footwall. **(b)** Concave-up hillslopes in valleys in the footwall of the Servia normal fault, suggesting recent and fast uplift.

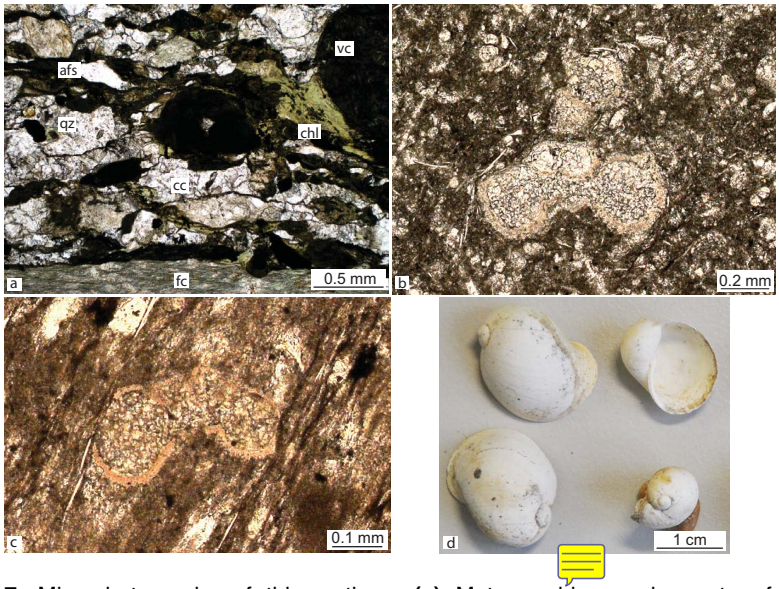

Figure 7. Microphotographs of thin-sections. **(a)** Metamorphic conglomerate of sample 10-029 with metamorphic chlorite (chl) in calcitic matrix. Other clasts: fc = felsic clast, afs = feldspar, qz = quartz and vc = volcanic clast. **(b)** Turonian *Helvetoglobotruncana helvetica* (93.5 and 90 Ma) in marls on the transgressive discordance. **(c)** Late Cretaceous (> 66 Ma) *Globotruncana sp.* in the marls incarlated with sample 10-128. **(d)** Pliocene to recent art *Radix Auriculata* found in the lacustrine sediments.

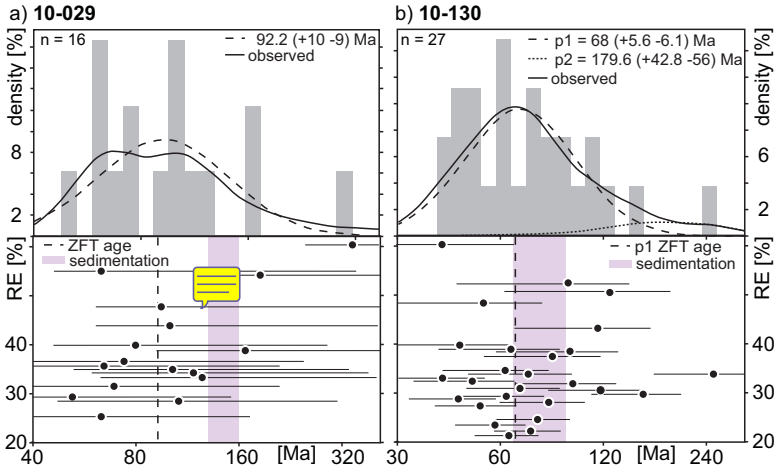

Figure 8. Age density histograms for "detrital" FT ages with distribution curves (n = number of grain measured, p = population, RE = relative error in %) calculated with Binomfit (Brandon, 1996). **(a)** Zircon age-distribution of grain-supported conglomerate 10-029 belonging to the Upper Malm–Lower Cretaceous "flysch" of the AVAZ (IGME, 1991). **(b)** Zircon age-distribution from unmetamorphosed, Late Cretaceous conglomerate (10-130).

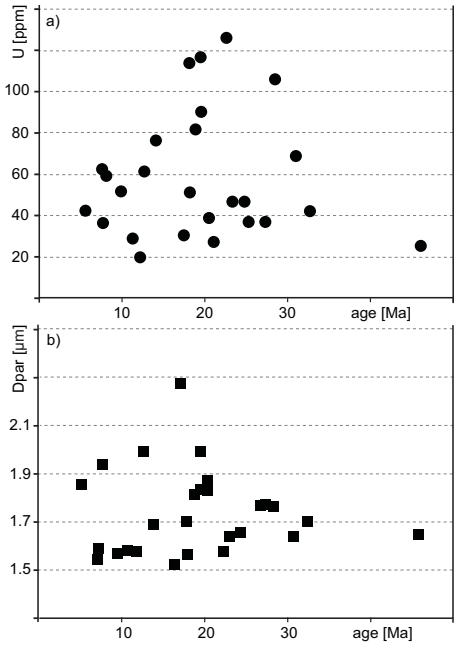

Figure 9. Plots of single apatite measurements of sample 09-055. **(a)** U-concentration vs. ages; **(b)** Dpar vs. age.

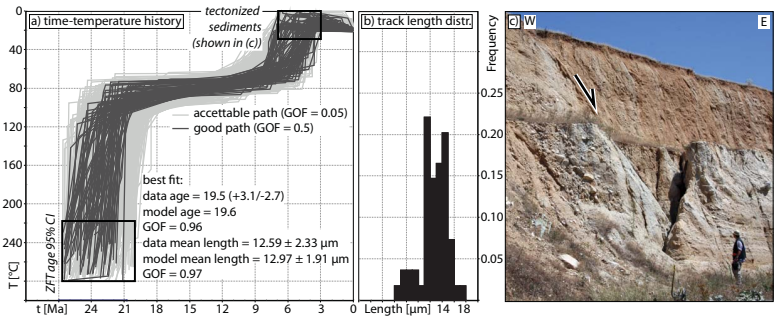

Figure 10. (a) T-t paths of sample 09-055 modeled with computer program HeFTy (Ketcham, 2005). The "acceptable" (> 0.05) and "good" (> 0.5) goodness-of-fit indicate non-failure at 95 and 50 % confidence interval, respectively. Inverse modeling is based on simulation of 50 000 random t-T paths. **(b)** Distribution of ~~counted~~ horizontal track lengths. **(c)** Normal fault in deltaic-lacustrine sediments (< 5 Ma) uncorformably covering the Pelagonia crystalline rocks (N40°19′49.4″, E022°08′33.5″).

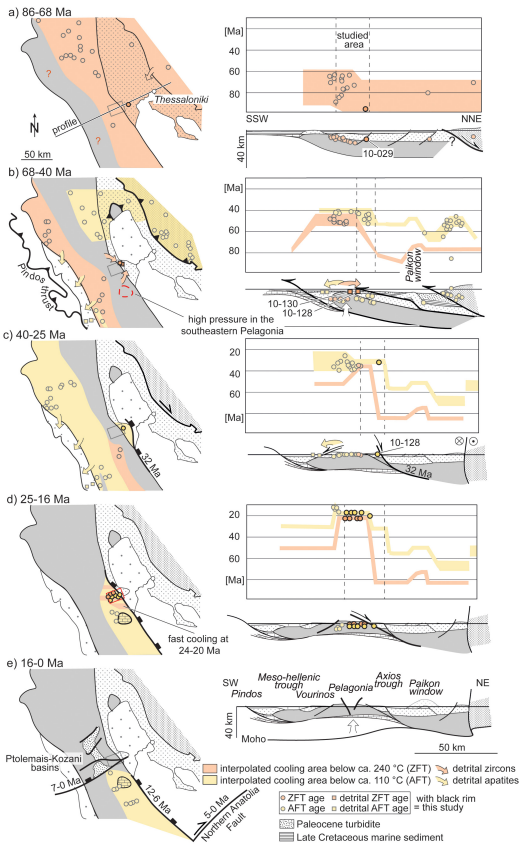

Figure 11. ZFT and AFT therma tory of the Pelagonia fro e Late Cretaceous with restored profiles. ZHe and AHe ages neglected since not homogenously distributed in the area. Unit patte identical to Fig. 1. Conceptual cooling terns along thrust sheets from Lock and Willett (2008). Until ca. 32 Ma, cooling homogeneous and parallel to the NW–SE tectonic contacts.

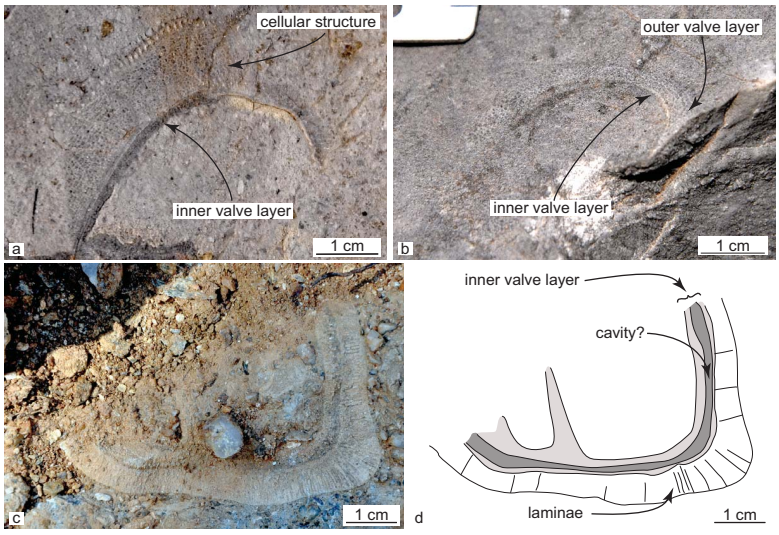

Figure A1. (a) composite shell of a rudist (*Durania*) (40°27′40.7″ 022°13′13.8″) **(b)** bi-layered shell of the *Radiolitidae* showing an external layer with polygonal ornaments (40°27′31.2″ 022°13′07.7″). **(c)** Multi-layer architecture of a Rudist shell fragment (*Plagioptychid*) in a conglomerate, showing radial laminae in the outer-valve layer (40°27′45.1″ 022°12′26.7″); **(d)** Sketch of the Rudist fragment shown in **(c)**.